A storage-based model of heterocyst commitment and patterning in cyanobacteria

Aidan I Brown and Andrew D Rutenberg[1]

Department of Physics and Atmospheric Science, Dalhousie University, Halifax, Nova Scotia, B3H 1Z9, Canada

E-mail: aidan@dal.ca, andrew.rutenberg@dal.ca and adr@dal.ca

Abstract

When deprived of fixed nitrogen (fN), certain filamentous cyanobacteria differentiate nitrogen-fixing heterocysts. There is a large and dynamic fraction of stored fN in cyanobacterial cells, but its role in directing heterocyst commitment has not been identified. We present an integrated computational model of fN transport, cellular growth, and heterocyst commitment for filamentous cyanobacteria. By including fN storage proportional to cell length, but without any explicit cell-cycle effect, we are able to recover a broad and late range of heterocyst commitment times and we observe a strong *indirect* cell-cycle effect. We propose that fN storage is an important component of heterocyst commitment and patterning in filamentous cyanobacteria. The model allows us to explore both initial and steady-state heterocyst patterns. The developmental model is hierarchical after initial commitment: our only source of stochasticity is observed growth rate variability. Explicit lateral inhibition allows us to examine $\Delta patS$, $\Delta hetN$, and $\Delta patN$ phenotypes. We find that $\Delta patS$ leads to adjacent heterocysts of the same generation, while $\Delta hetN$ leads to adjacent heterocysts only of different generations. With a shortened inhibition range, heterocyst spacing distributions are similar to those in experimental $\Delta patN$ systems. Step-down to non-zero external fN concentrations is also investigated.

S Online supplementary data available from stacks.iop.org/PhysBio/11/016001/mmedia

1. Introduction

Certain filamentous cyanobacteria are model multicellular organisms that, under conditions of low exogenous fixed nitrogen (fN), terminally differentiate regularly spaced heterocysts that fix nitrogen for interspersed clusters of photosynthetic vegetative cells. While much is known about the genetic regulation of heterocyst development [1, 2], the mechanism by which certain cells are selected to become heterocysts has nevertheless remained mysterious.

There are prompt signs of nitrogen deprivation after the step-down of fN, such as the activation of nitrate assimilation genes [3] and the increase of 2-oxoglutarate levels [4] within 1 h. After this, there is a long delay until 8 h to 14 h after the fN step-down, when the first generation of cells commit to become heterocysts [5]. Rapid diffusion of calcein, a non-native fluorescent reporter, has been observed in filamentous cyanobacteria [6]. This suggests that the diffusion of small molecules carrying fN along the filament will also be rapid [7], and that commitment may be influenced by more than the depletion of diffusible fN alone.

Suggestions that heterocyst differentiation is strictly dependent on the cell cycle [8, 9] have not been borne out by

---

[1] Author to whom any correspondence should be addressed.

experiment [10, 11]. However, unicellular studies show that cell size can affect cell fate decisions without explicit cell-cycle effects, for example in yeast meiosis [12] or in phage lambda infection [13]. While postulated mechanisms of cell size effects vary, they include nutrient availability [13]. In the multicellular cyanobacterial system, substantial stores of fN are available. Cyanophycin and phycobiliprotein represent up to 20% [14] of protein and 60% [15] of soluble protein, respectively, and are depleted under fN limitation [16]. Could there be a role for fN storage, involving cell size, in heterocyst commitment?

Buikema and Haselkorn [17] suggested that uneven accumulation of cyanophycin would cause some cells to starve first, leading to commitment variability, but reported no evidence of uneven accumulation of cyanophycin along the filament. However, a uniform concentration (per unit volume) of fN storage combined with the natural diversity of cell sizes in growing filaments would lead to uneven total fN storage per cell along the filament—because length and hence volume would vary from cell to cell.

We explore the hypothesis that an initially uniform concentration of fN storage could explain the timing and variability of initial heterocyst commitment in *Anabaena* PCC 7120. We do this within the context of a computational model of filament growth and development that allows for fN storage, transport, and consumption by cell growth. We impose a deterministic, or hierarchic [18], developmental schedule that committed cells follow to become heterocysts. This deterministic schedule ensures that the only stochastic event in heterocyst development is the time of commitment. In particular the model allows for no intrinsic variability in lateral inhibition due to *patS* [5, 19] and *hetN* [20]. Developmental and systems-biology studies of cyanobacterial filaments need to account for the population context of cells [21], and the model indicates that the total fN storage of each cell may be an important source of variability determining which cells differentiate into heterocysts.

We can use the model to examine how the heterocyst pattern changes with time—from the initial commitment to the spacing distribution at 24 h and 48 h after fN step-down. We find that uniform storage together with a natural distribution of cell lengths is enough to provide a strong *indirect* cell-cycle effect on committed heterocysts, with shorter cells favored for heterocyst differentiation [8, 9]. We obtain the observed 8–14 h timing and range of commitment seen in experiments [5], and predict that both storage fraction and growth rate should control overall commitment timing.

The model also recovers the multiple-contiguous heterocyst (Mch) phenotype and timing of both Δ*patS* [5, 19] and Δ*hetN* [20] knockouts—and predicts that clusters of heterocysts seen in Δ*hetN* filaments will always include distinct generations of heterocysts, and so will be qualitatively distinct from heterocyst development in Δ*patS* filaments. The model is used to show that heterocyst patterning effects similar to those of Δ*patN* [22] can be obtained by simply reducing the inhibition range of *patS* and *hetN*.

Some heterocystous cyanobacterial filaments fix nitrogen in vegetative cells under anoxic conditions, and yet still differentiate heterocysts in a pattern [23]. Under the assumption that such vegetative fixation provides a background level of fN that is not quite sufficient for maximal vegetative growth, we also investigate heterocyst differentiation when the nitrogen steps down to nonzero external fN concentrations. These conditions could be accessed in developmental studies using flow chambers.

2. Computational model

An early quantitative fN transport and consumption model by Wolk *et al* [24] considered how fN would spread from a heterocyst to surrounding vegetative cells, but did not include distinct cells or stochasticity and assumed that fN was always rate-limiting for growth. Allard *et al* [25] considered dynamic heterocyst placement in growing, stochastic filaments of cells with fN transport but only used periplasmic transport without inhibitors. Their fN dynamics was adapted for cell–cell transport by Brown and Rutenberg [7], who demonstrated that a constant cell growth rate in the presence of fN was consistent with observed nitrogen distributions between two heterocysts. This model was extended to the filament level [26] to recover heterocyst spacing distributions during steady-state growth. These models suggest that fN dynamics are important for steady-state heterocyst patterns, but could not address the initial heterocyst patterns observed soon after fN step-down since they did not explicitly include lateral inhibition due to, e.g., *patS* and *hetN*.

Earlier modeling efforts showed that initial heterocyst patterns were not random [27] but were consistent with diffusible inhibitors [28]. These models did not include growth, fN transport, or distinct effects of *patS* and *hetN*. Recently, an integrated local model with static heterocysts has been presented [29]—but without stochasticity it is unable to address heterocyst pattern formation at the filament level.

In this work we implement a stochastic computational model of the cyanobacterial filament, focusing on the model organism *Anabaena* PCC 7120. The model has growth, division, and fN transport, along with dynamic heterocyst placement using storage-based commitment and explicit lateral inhibition of differentiation. Our quantitative heterocyst differentiation model is similar in spirit to the qualitative proposal by Meeks and Elhai [27] of a two-stage model of heterocyst differentiation with biased initiation based on the cell cycle followed by competitive resolution of differentiating clusters to isolated heterocysts. The crucial difference is that the model we propose includes local fN storage, which we use to initiate development instead of an explicit cell-cycle effect. Since we have growth, fN dynamics, and explicit lateral inhibition due to *patS* and *hetN* in a stochastic developmental model we can calculate both initial and steady-state heterocyst patterns and compare them with experimental distributions.

2.1. Fixed nitrogen transport

The dynamics of freely diffusing fN, N_i, are given by

$$\frac{dN_i}{dt} = \Phi_i + D_I \rho_{efN} l_i - D_L N_i + G_i, \tag{1}$$

where $\Phi_i \equiv \Phi_R(i-1) + \Phi_L(i+1) - \Phi_R(i) - \Phi_L(i)$ is the net diffusive flux into cell i. Each flux is the product of the local density N_i/l_i, where l_i the length of cell i, and a transport coefficient D_C which accounts for the flux magnitude and absorbs all geometric factors. We use $D_C = 1.54\ \mu\text{m s}^{-1}$ between two vegetative cells and $D_C = 0.19\ \mu\text{m s}^{-1}$ between a vegetative cell and a heterocyst [7]. The import from outside the filament is expected to be proportional to the number of transporters, which will be proportional to the cell surface area and thus the cell length for cylindrical cells. Import is then proportional to the cell length, the coefficient $D_I = 2.9 \times 10^{-18}\ \text{m}^3(\mu\text{m s})^{-1} = 1.7 \times 10^9\ \text{M}^{-1}(\mu\text{m s})^{-1}$, which has geometric factors included, and the external fN concentration ρ_{efN} [26]. We also allow a small leakage, which is expected to be proportional to cytoplasmic density, $N/(Al)$, with A the cross-sectional area, but also the number of transporters, which is expected to be proportional to cell length l. This results in a leakage term independent of cell length and proportional to the amount of fN N and the coefficient $D_L = 0.029/\pi\ \text{s}^{-1}$ (geometric factors are absorbed) [26]. G_i is a source/sink term and is described below.

2.2. Cell growth and division

Following [26], we take *Anabaena* PCC 7120 cells to have a minimum size of $l_{\min} = 2.25\ \mu\text{m}$ and a maximum size of $l_{\max} = 2l_{\min}$ [1, 2]. When a cell reaches $l_{\max}$ it is divided into two cells of equal length, each of which is randomly assigned a new growth rate and half of the fN and fN storage of the parent cell. Daughter cells assigned different growth rates will have different lengths at later times and so lead to a natural population structure with diverse cell lengths. To select a new growth rate we first define a minimum doubling time $T_{\min} = T_D - \Delta$ and a maximum doubling time of $T_{\max} = T_D + \Delta$, with an average doubling time $T_D = 20$ h [30] and a range $\Delta = 4.5$ h [26] that preserves the reported experimental coefficient of variation [25]. A doubling time T_i is randomly and uniformly selected from its range and converted to a maximal growth rate $\hat{R}_i = l_{\min}/T_i$.

Single cell growth rates have not been reported in cyanobacteria. However the length increase of individual *E. coli* cells is approximately linear in time [31]. Accordingly, our model assigns each individual cell a constant maximal growth rate. The actual growth rate, R_i, is at most $\hat{R}_i$ but is reduced if the local availability of fN is insufficient to accommodate maximal growth [26]:

$$R_i = \begin{cases} \hat{R}_i & N_i > 0 \\ \min(\Phi_{\text{in}}/g + f_g\hat{R}_i, \hat{R}_i) & N_i = 0, N_{Si} > 0 \\ \min(\Phi_{\text{in}}/g, \hat{R}_i) & N_i = 0, N_{Si} = 0 \end{cases} \quad (2)$$

where g is the fN cost per unit length of growth, f_g is the fraction of the maximal growth rate $\hat{R}$ that can be accommodated by stored fN, and N_S is the amount of stored fN. The first condition imposes that any cytoplasmic fN can accommodate the maximal growth rate; the second condition that local storage can accommodate up to $f_g\hat{R}_i$ of growth; the last two conditions that any influx of fN from neighboring cells and

outside the filament, Φ_{in}, will immediately accommodate some growth when $N_i = 0$. For vegetative cells

$$G_i = G_{\text{veg}} = \begin{cases} -gR_i & N_i > 0 \\ -\Phi_{\text{in}} & N_i = 0. \end{cases} \quad (3)$$

For simplicity, the model allows for vegetative growth even for vanishingly small N_i. A minimum threshold concentration for growth could be easily included, though we do not anticipate significant changes as long as the threshold is small compared to the cellular fN growth requirement per unit length, g.

2.3. Fixed nitrogen storage

Each cell i has an amount of stored fN, N_{Si}, that provides fN for the cell to grow when the diffusible cytoplasmic fN, N_i, has run out. Storage is composed of cyanophycin and phycobiliprotein, and this storage is degraded upon nitrogen deprivation [16]. Once heterocysts have developed, cyanophycin is replenished in both vegetative cells and heterocysts [32]. In the model, a fraction f_s of the fN incorporated by the cell will be storage (we use $f_s = 0.3$, see section 2.4). This then gives us the fN storage dynamics of the ith cell:

$$\frac{\text{d}N_{Si}}{\text{d}t} = \begin{cases} f_s g R_i & N_i > 0 \\ f_s \Phi_{\text{in}} - (gR_i - \Phi_{\text{in}}) & N_i = 0, \end{cases} \quad (4)$$

where g is the fN cost per unit length of growth, R_i is the growth rate of the ith cell, and Φ_{in} is the influx of fN into the ith cell from adjacent cells and from outside the filament. For simplicity, we assume that only enough stored fN for local growth needs is released in equation (4). This released fN is immediately taken up by local growth, and none is available for diffusion to other cells. Storage regenerates when diffusible fN is available, with all cells gaining the same amount of storage per unit length grown when $N_i > 0$. A filament that has been grown indefinitely in excess fN will have cells with the same amount of storage per unit length, $f_s g$, while cells that have been starved will have less than this amount. If a cell is starved and then returned to excess fN, then its fN storage density will asymptotically approach $f_s g$.

In the model, the initial cytoplasmic fN concentration upon fN step-down is set so that cytoplasmic fN is exhausted in all cells within the first hour (see bottom-right inset of figure 1). This is consistent with the activation of nitrate assimilation genes [3] and increase in 2-oxoglutarate levels [4] within 1 h of nitrogen deprivation. Nevertheless, ongoing growth of cyanobacterial filaments is observed experimentally well after this time (see top-left inset of figure 1)—though it is reduced by a factor of $f_g \approx 0.25$ compared to later times after mature heterocysts are supplying newly fN [10]. We find that utilization of fN storage is essential to recover this ongoing growth (see figure 1). We also incorporate the experimental observation that division lags even behind the reduced growth in filament length for approximately the first 24 h [10] with a requirement that cells divide only when they have non-zero levels of cytoplasmic fN, i.e. $N_i > 0$. As shown in figure 1, after mature heterocysts have developed and begin to produce fN at ≈ 18 h, division resumes and the filament resumes rapid growth.
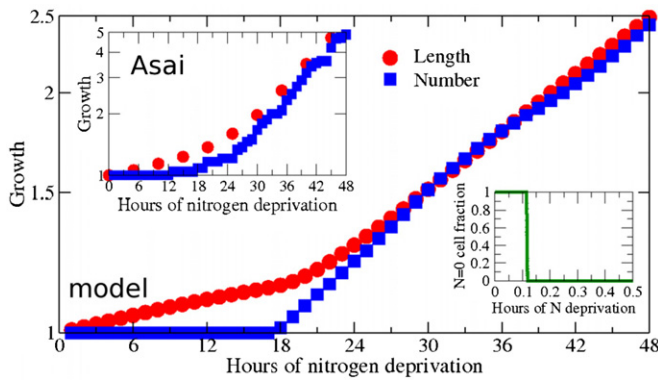
Figure 1. Growth of length (red circles) or number of cells (blue squares), relative to the initial values, of cyanobacterial filament versus time since the start of fixed nitrogen deprivation. The top-left inset is experimental data digitized by hand from Movie S1 in Asai *et al* [10], while the main figure shows the computational model results. As described in the text, model division is suppressed when diffusible fixed nitrogen is unavailable—though reduced growth is still allowed at the expense of fN storage. The bottom-right inset shows the fraction of model cells with zero cytoplasmic, diffusible fixed nitrogen ($N_i = 0$). Just after $t = 0.1$ h the filament rapidly changes from all cells with $N_i > 0$ to all cells with $N_i = 0$.

2.4. Estimation of storage fraction, f_s

To estimate the storage fraction, f_s, we separately estimate the amounts of nitrogen contained in reserves of cyanophycin and phycobiliprotein in vegetative cells. PCC 7120 has 636 μg arginine/mg chlorophyll, while a cyanobacterial species that does not synthesize cyanophycin has 68 μg arginine/mg chlorophyll, so we estimate that 568 μg arginine/mg chlorophyll is from cyanophycin [32]. Cyanophycin is 1:1 arginine:aspartic acid, where arginine has four nitrogen atoms and aspartic acid has only one, so there are approximately five nitrogen atoms in cyanophycin for every arginine from cyanophycin. *Anabaena cylindrica* has 0.58 μg chlorophyll/10^6 cells, but its cells are 2.25 times as large as those of PCC 7120 [7], so we estimate that PCC 7120 has 0.26 μg chlorophyll/10^6 cells. Together, 568 arginine/mg chlorophyll × 5 N atoms per arginine × 0.26 μg chlorophyll/10^6 cells gives 2.55×10^9 nitrogen atoms in cyanophycin per cell. There are 2.07×10^{10} nitrogen atoms per cell in PCC 7120 [7] and so 12.3% of the nitrogen atoms are in cyanophycin. This ballpark estimate for the amount of cyanophycin is comparable to, though somewhat below, measurements of a maximum of 20% of protein in *Cyanothece* sp. ATCC 51142 [14]. Accordingly, we use a value of 15% of the fN in the cell in the form of cyanophycin. Phycobiliprotein can comprise up to 60% of the soluble protein in a cell [15] and upon nitrogen deprivation is observed to partially degrade in cells that remain vegetative [33]. We choose another 15% of the total fN in the cell to be storage in the form of phycobiliprotein that is available for growth upon nitrogen starvation. This gives a total of 30% of the fN as storage available for growth, and we assign $f_s = 0.3$. Other values of f_s will lead to similar results, with the caveat that at least one of growth rate ($f_g \hat{R}$), fN requirements of growth (g), or the commitment threshold (see next section) would also need to be adjusted to retain the experimentally observed commitment timing.
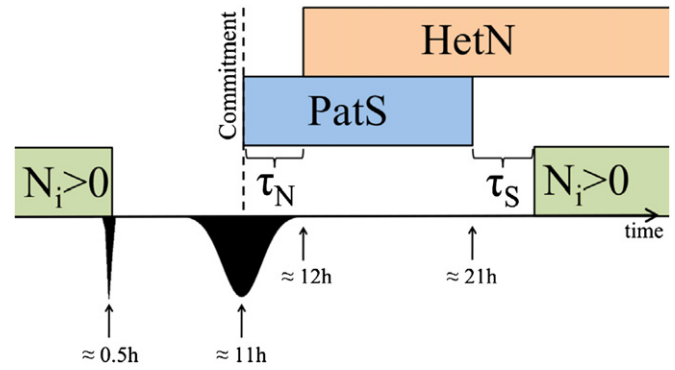

Figure 2. Heterocyst commitment and differentiation model for cells that commit to become heterocysts. Indicated times are measured from the onset of extracellular fixed nitrogen (fN) deprivation. Cytoplasmic fN (green bar on lower left) runs out relatively quickly, after less than 0.5 h. In the model, the cell-to-cell variability of the timing of this depletion is relatively narrow, illustrated by the narrow black inverted peak at the lower left. The cells then rely on stored fN for ongoing growth. Since stored fN is not shared between cells, it is significantly depleted at quite different times in different cells—as represented by the broad black inverted peak centred at 11 h. When storage is significantly depleted, heterocyst commitment occurs—as indicated by the vertical dashed line for a cell that commits at 11 h. Upon commitment, lateral inhibition due to *patS* (blue bar) occurs immediately. Lateral inhibition due to *hetN* (orange bar) starts after a delay τ_N and is ongoing. PatS inhibition stops at heterocyst maturity (10 h after commitment), and after a delay τ_S the mature heterocyst is fixing significant amounts of diffusible fN (green bar on lower right). The inhibitory effects of PatS and HetN have a fixed range of five cells, in both directions, from the inhibiting cell.

2.5. Heterocyst commitment

The cyanobacterium *Aphanocapsa*, when deprived of external fN, first consumes cyanophycin, then phycobiliprotein [16]. Vegetative cells only ever transiently and incompletely deplete their phycobiliprotein, as it participates in ongoing photosynthesis [33]. We follow this phenomenology and commit cells to become heterocysts when the available stored nitrogen is half of its maximal level, i.e. $N_{Si} < 0.5 f_s g l_i$ (l is cell length)—unless lateral inhibition (see below) prevents commitment. Note that the precise threshold fraction used, like the fraction of fN represented by storage (f_s), does not change the qualitative results—but does move the average timing of commitment earlier or later. Nevertheless, commitment triggered at 50% of local storage roughly corresponds to local exhaustion of cyanophycin storage. Such local exhaustion may indicate a biological mechanism for heterocyst commitment.

Committed heterocysts do not grow in the model, i.e. $R_i = \hat{R}_i = 0$. Rather they enter a deterministic developmental process. The stochastic nature of heterocyst commitment, in the model, arises entirely from the stochastic timing of stored nitrogen depletion (at approximately 11 h, but broadly distributed, as illustrated by the broad inverted peak at the bottom of figure 2). We assume that after a cell commits to differentiation it will take 10 h to mature developmentally (as indicated by the blue bar in figure 2). This 10 h interval is the delay seen in PCC 7120 between the 8–14 h range of commitment [5] and the 18–24 h expression of nitrogenase [34]. This is also approximately the same delay seen in

Anabaena cylindrica between the earliest commitment at 5 h and the earliest mature heterocysts at 14 h [33]. We also allow for a delay τ_S between maturity and significant production of fN . We explore the effects of varying τ_S (see results). After this delay, mature heterocysts fix nitrogen at a rate $G_i = G_{het} = 3.15 \times 10^6$ s^{-1} [26], as indicated by the green bar at the bottom-right of figure 2.

2.6. Lateral inhibition

Heterocysts produce both PatS and HetN to laterally inhibit nearby cells from committing to become heterocysts. Both gene products are thought to be processed into a diffusible peptide [19, 35]. *patS* acts early and affects the initial selection of cells for heterocyst development after fN deprivation [5, 19]. *hetN* acts later [36] and affects steady-state heterocyst patterns only after approximately one day of fN deprivation [20].

To highlight the role of fN storage, we have simplified the detailed dynamics of PatS and HetN [29] so that in the model the inhibition from a given cell is either on or off, i.e. it is represented by a Boolean model [37]. Similarly, the inhibition effect is given a fixed range—reflecting the fixed range found experimentally in filamentous cyanobacteria [8]. For simplicity, and because inhibition by PatS and HetN may involve the same peptide [38], we use the same range for the effects of *patS* and *hetN*. Reported experimental heterocyst frequencies at 24 h include 7.8% [9], 9.1% [11], and 10.4% [5]. For the model, heterocyst frequency at 24 h decreases as the inhibition range increases: an inhibition range of three cells gives an 11.6% frequency, four cells 10.1%, five cells 8.7%, and six cells 7.6%. Accordingly, unless otherwise noted we choose an intermediate inhibition range of 5, which also agrees with the range reported by Mitchison *et al* [8] for *Anabaena catenula*. The effects of inhibition due to *patS* or *hetN* from a given cell are the same—within the finite inhibition range no other cells will commit to becoming heterocysts. Those inhibited cells will continue to grow and divide, subject to available fN. Inhibition has no effect on already committed cells, or on mature heterocysts.

We have used a hierarchic [18], or deterministic, model of inhibition timing. As illustrated by the blue bar in figure 2, the inhibition due to *patS* begins at commitment and ends (10 h later) at heterocyst maturity. Inhibition due to *hetN* is similar, but begins a time τ_N after commitment and does not end. Since the timing of commitment of individual cells can vary considerably, the timing of significant lateral inhibition from a given cell will correspondingly vary—but the model has no stochasticity for the developmental process of an individual cell after commitment.

There are three inhibitory products of committed cells. The first is PatS; after a delay τ_N, the next is HetN; and a time τ_S after the *patS* turns off, newly synthesized fN inhibits commitment near the new heterocyst. In wild-type (WT) cells, these inhibitory signals overlap in time. Later, we will use the model to explore the effects of $\Delta patS$ and $\Delta hetN$ mutants in which inhibition of nearby cells is no longer uninterrupted after commitment. We will also explore the hypothesis that heterocyst patterns similar to the recently reported $\Delta patN$

phenotype can be recovered by simply reducing the inhibition range. All of the model results shown in this paper use short delays, with $\tau_N = \tau_S = 1$ h. We discuss (below) the sensitivity of the results on those delay times.

2.7. Further numerical details

For fN transport between cells, periodic boundary conditions were used to minimize end effects. Filaments were initiated as a single cell with zero cytoplasmic fN and with maximum storage, $N_S = f_s gl$, in a high concentration of external fN. After seven days of growth in high external fN, to generate a random population structure of cell lengths, the external fN concentration was stepped down (to zero unless otherwise stated) and the amount of cytoplasmic nitrogen was set to 5% of the current fN content incorporated into the cell, $0.05gl_i$, so that the depletion of cytoplasmic fN is prior to the 0.5 h time at which nitrate assimilation genes are activated [3]—one of the earliest signs of nitrogen deprivation.

Filament length and mature heterocyst frequency were recorded every hour. Heterocyst spacing distributions were recorded at the indicated times. Times are reported with respect to when the external fN concentration was stepped down. Commitment was measured similar to the experimental technique of Yoon and Golden [5], where nitrate was added to the medium at a certain time and the subsequent heterocyst frequency at 24 h is reported: in the simulation the external fN level was changed to a high concentration at the indicated time, and the filament allowed to grow until the heterocyst frequency was recorded at 24 h.

Table 1 summarizes parameter values used in this paper.

3. Results and discussion

3.1. Commitment timing

The filament is deprived of external fN at 0 h. As the cells starve of fN some commit to develop into heterocysts—following the deterministic developmental program outlined in figure 2. Experimentally, commitment is assessed by raising the external fN to a high concentration after a delay [5, 33] and measuring the resulting heterocyst fraction at 24 h. In PCC 7120, if the delay is shorter than around 8 h no cells commit, while if longer than around 14 h then the normal number of cells commit [5]. As shown in figure 3(*a*) with the red circles, we recover the same qualitative commitment curve with the model.

The variation of commitment timing is determined by the fN storage. In the model, commitment begins only after the first cells have depleted half of their stored fN. Because the maximum nitrogen storage is a fixed fraction f_s of the cellular content, this occurs first in the smallest and in the fastest growing cells. Cells will continue to commit until all cells have either committed to differentiation or been blocked by lateral inhibition. Because of the distribution of cellular stored fN and growth rates, commitment does not slow until about 14 h. After that, there is little further commitment until the first mature heterocysts provide newly fN at 19 h.

Table 1. Model parameter definitions and values. Shown are the standard values used. Further discussion is found in section 2.

Variable	Description	Value/Equation
N_i	Cytoplasmic fN amount of cell i	Variable
N_{Si}	Stored fN amount of cell i	Variable
Φ_i	Diffusive flux from neighboring cells to cell i	Variable
Φ_{in}	Influx of fN from neighbors and outside filament	Variable
ρ_{efN}	External fN concentration	Varied
D_C	Coefficient for vegetative cell to vegetative cell fN transport	$1.54~\mu\text{m s}^{-1}$
D_I	Coefficient for fN import from external fN	$2.9 \times 10^{-18}~\text{m}^3(\mu\text{m s})^{-1}$
D_L	Coefficient for fN leakage	$0.029/\pi~\text{s}^{-1}$
G_i	Source/sink term related to fN production/growth	Variable
G_{veg}	Cytoplasmic fN removed to support vegetative growth	Equation (3)
G_{het}	Heterocyst fN production	$3.15 \times 10^6~\text{s}^{-1}$
l_i	Length of cell i	$[l_{min}, l_{max}]$
l_{min}	Minimum length of cell	$2.25~\mu\text{m}$
l_{max}	Cell length triggering division	$4.5~\mu\text{m}$
T_i	Doubling time of cell i	$[T_{min}, T_{max}]$
T_{min}	Minimum cell doubling time	$T_D - \Delta$
T_{max}	Maximum cell doubling time	$T_D + \Delta$
Δ	Range of cell doubling times	$4.5~\text{h}$
T_D	Average cell doubling time	$20~\text{h}$
R_i	Growth rate of cell i	Equation (2)
$\hat{R}_i$	Maximal growth rate of cell i	l_{min}/T_i
g	fN cost per unit length of growth	$6.2 \times 10^9/\mu\text{m}$
f_g	Maximal growth rate fraction provided by stored fN	0.25
f_s	Fraction of fN used to grow that is stored	0.3
τ_N	Delay after het commitment until HetN inhibition begins	Varied
τ_S	Delay after end of PatS inhibition until fN production begins	Varied

With storage-based commitment we predict that filaments with faster growth rates will deplete their storage faster and commit to differentiation earlier. Bradley and Carr found earlier commitment in *Anabaena cylindrica*, ranging between 5–10 h [33]. Their doubling time for growth was 16.4 h, shorter than a typical PCC 7120 generation time of about 20 h [30]. As shown in figure 3(*a*), we find that with a 50% faster growth rate the commitment curve started at 6 h—consistent with Bradley and Carr [33]. It has also been observed experimentally that increasing light intensity, which results in increased growth rate, causes earlier heterocyst differentiation (see figure S7 of [11]). Decreasing the amount of storage in our model produces a similar effect (see figure S1 in the supplementary material, available from stacks.iop.org/PhysBio/11/016001/mmedia), which may also contribute to the earlier commitment seen in *A. cylindrica*.

3.2. Cell-cycle effects

While the cell cycle does not strictly regulate heterocyst commitment [10, 11], some association between the two has been reported [8, 9]. Since the model does not explicitly require that a cell is in a certain stage of the cell cycle to commit to heterocyst differentiation, we can use it to explore possible indirect effects of cell cycle on heterocyst commitment.

Diffusible fN runs out for all cells in a narrow range of time (see figure 1, bottom-right inset) because of the rapid rate of diffusion along the filament. After the diffusible fN has run out, all cells will grow using stored fN and smaller cells, having less storage, are on average expected to deplete storage sooner. Statistics on the length of the cell at the time of

commitment are shown in figure 3(*b*). Cells double in length between birth and subsequent division: we take this fractional growth to define a cell-cycle between 0%–100% extension. We see at 24 h (red circles) that shorter cells, which are earlier in the cell cycle, are more likely to commit to heterocyst differentiation. This suggests there may be an indirect effect of cell cycle on heterocyst commitment. Interestingly, because even the shortest and fastest growing cells do not exhaust their storage immediately, the peak is not immediately after division. The cell-cycle effect is less pronounced at 48 h, since only vegetative cells close to midway between existing heterocysts have a chance to exhaust their nitrogen storage [7].

3.3. Change of heterocyst frequency with time

The frequency of mature heterocysts in wild-type filaments at different times after nitrogen deprivation, shown as the red circles of figure 3(*c*), is similar to the commitment curve—but delayed by 10 h to allow for maturation. However, since exogenous fN is not reintroduced, the heterocyst frequency can be followed well after 24 h. We see that the first heterocysts mature after 19 h and the heterocyst frequency increases rapidly for several hours. This is consistent with the maturity of first generation heterocysts after 18–24 h of nitrogen deprivation [34, 39]. After 24 h the heterocyst frequency oscillates, with a period of approximately 20 h, while it slowly drops from a peak of nearly 10% at 42 h to less than 9% at 96 h. Both the oscillation and decline of the heterocyst frequency have been observed in *Anabaena cylindrica* [33]. In the model, the slight decline is due to dilution of the original burst of heterocysts with ongoing growth, while the oscillations are due
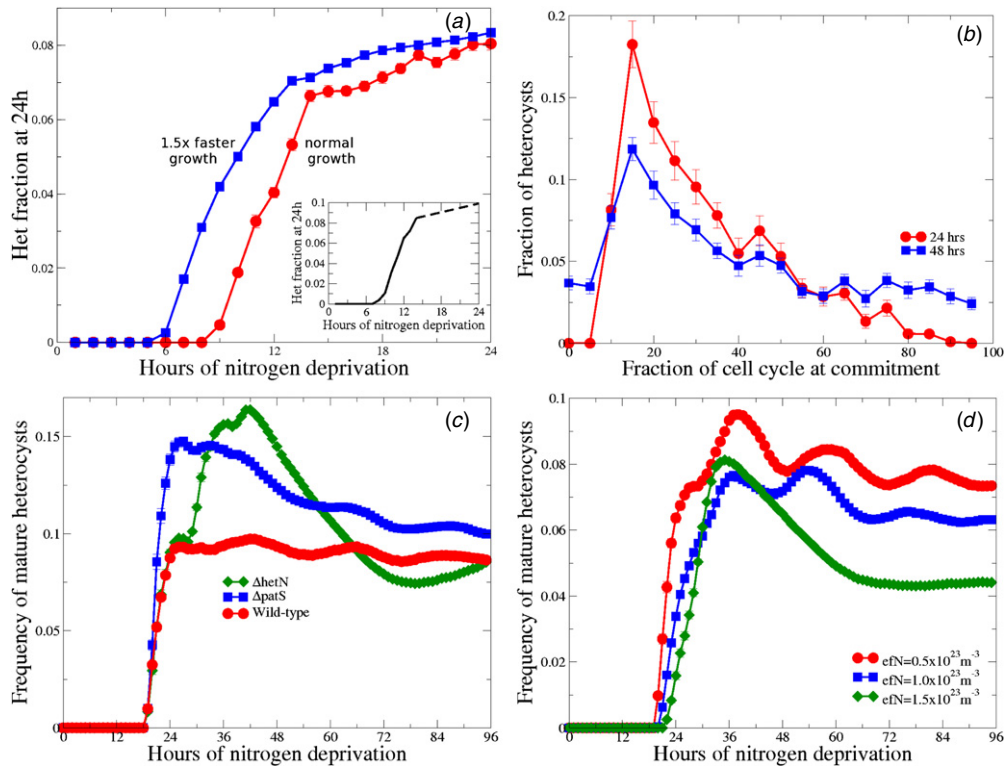
Figure 3. (*a*) Commitment curve of heterocyst fraction 24 h after the onset of nitrogen deprivation versus duration of nitrogen deprivation. Red circles are for a normal 20 h doubling time, while the blue squares shows commitment fraction when the growth rate is increased by 50%. Inset shows average of two sets of experimental data from Yoon and Golden [5] interpolated data to the point at 24 h, representing uninterrupted deprivation, is shown with a dashed line. (*b*) Indirect cell-cycle effect, illustrated by the distribution of the cell sizes that heterocysts had at commitment. Legend indicates time since nitrogen deprivation, either 24 h (red circles) or 48 h (blue squares). (*c*) The change of heterocyst frequency with time after nitrogen deprivation for wild-type (red circles), $\Delta patS$ (blue squares), and $\Delta hetN$ (green diamonds) filaments. (*d*) The change of heterocyst frequency with time after nitrogen step-down for wild-type, with step-down to ρ_{efN} (see equation (1)) of 0.5×10^{23} m^{-3} (red circles), 1.0×10^{23} m^{-3} (blue squares), and 1.5×10^{23} m^{-3} (green diamonds).

to the periodic enrichment of small daughter cells produced in subsequent waves of cell division due to growth that follows the provision of fN by newly mature heterocysts.

3.4. Heterocyst spacings

The distribution of the number of cells separating mature heterocysts characterizes the developmental pattern. The heterocyst spacing distributions after 24 and 48 h of nitrogen deprivation are shown for the model in figures 4(*a*) and (*b*) and for two experimental studies of PCC 7120 in figures 4(*c*)–(*f*).

The model distribution for 24 h has a peak at 8–10 cells, and is skewed to the left. At higher spacings, the distribution tails off gradually. At smaller spacings, there is a sharp cutoff at the inhibition range. The sharpness of the cutoff is an artifact of the model's simple fixed inhibition range of five cells. The spacing distribution evolves with time, and at 48 h the mean spacing has increased and the distribution has become more symmetric. We see similar behavior in the experimental distributions: asymmetric left-skewed distributions at 24 h, with smaller asymmetry but larger mean at 48 h. We also see considerable variation between the experimental distributions, indicating significant systematic variability of experimental conditions, which precludes a more detailed comparison with the model.

The model of commitment and lateral inhibition, figure 2, captures both the distribution of spacing of heterocysts and the change of that distribution with time. The only source of stochasticity in the model is a modest variation of growth rates between cells [7, 25], which is necessary to obtain a normal population structure of cells. Other sources of stochasticity do not appear to be necessary to understand the broad, qualitative features of the heterocyst spacing distribution and its change with time.

3.5. Heterocyst spacings with $\Delta patS$

Figures 5(*a*) and (*b*) show that experimental heterocyst spacing distributions without inhibition due to *patS* [5] are dramatically changed compared with wild-type (WT) experimental distributions. At 24 h approximately 25% of the heterocysts spacings are zero, or Mch, and non-zero spacings are shorter overall [19]. At 48 h the distribution of non-zero intervals is qualitatively similar to WT, however the fraction of Mch clusters was not reported and so is represented by an unfilled bar [5].

Since local lateral inhibition is explicit in the model, we can investigate heterocyst patterns without *patS*. We see from figure 2 that with $\Delta patS$, committed heterocysts still laterally inhibit with *hetN* but only after a delay of duration τ_N. We find (see figure S2 in the supplementary material, available from
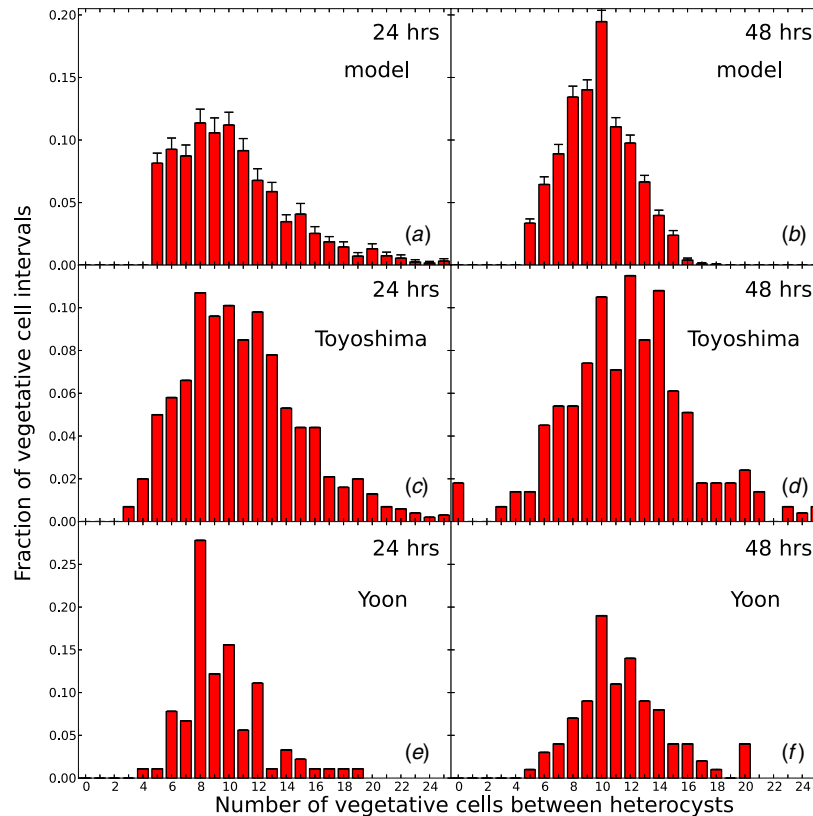
Figure 4. Wild-type (WT) heterocyst spacing distributions. (*a*) and (*b*) spacing distribution at 24 h and 48 h, respectively, using the model. Statistical error bars are shown. (*c*) and (*d*) spacing distribution from Toyoshima *et al* [11] at 24 h and 48 h, respectively. (*e*) and (*f*) spacing distribution from Yoon and Golden [5] at 24 h and 48 h, respectively, where we note that spacings of 20 also include counts from all greater spacings.

stacks.iop.org/PhysBio/11/016001/mmedia), that increasing τ_N increases the fraction of heterocyst clusters. We use $\tau_N = 1$ h and recover the $\approx 25\%$ Mch fraction seen experimentally at 24 h [5]. The model results, in figures 5(*c*) and (*d*), show the qualitative features seen experimentally: the shift toward lower spacings at 24 h and the return of a qualitatively WT pattern of non-zero intervals at 48 h. The recovery of the distribution toward WT is partly caused by the production of fN by mature heterocysts. It is also due to HetN inhibition, which although later than the PatS inhibition, still restricts further commitment. Existing heterocyst clusters are diluted but not destroyed by ongoing growth and division of vegetative cells. The model indicates that more heterocysts commit after 24 h, increasing the number of Mch clusters slightly more than they are diluted, so that at 48 h the Mch fraction is still approximately 25%.

The remaining heterocyst clusters also lead to an enhanced heterocyst frequency, as shown by blue squares in figure 3(*c*). The heterocyst frequency for $\Delta patS$ initially rises from zero at 19 h, the same time as WT, but peaks at a significantly higher frequency of 14.8% due to the lack of PatS inhibition. The percentage then slowly decreases toward the WT value, because the extra heterocysts limit nitrogen starvation and therefore new heterocyst differentiation. Experimental heterocyst percentages versus time for $\Delta patS$ *Anabaena* PCC 7120 also show elevated heterocyst percentages ($\sim$20%) that also appear to oscillate as time passes [40].

Experimental $\Delta patS$ heterocyst percentages are higher than those from the model. We believe that this is due to

the absence of carbohydrate dynamics in the model, so that when heterocyst percentages are elevated above WT we miss the expected reduction of fN production per heterocyst due to carbohydrate restriction [41]. This effect is also seen with $\Delta hetN$ strains (see next section). We expect this to be an even more significant issue with the heterocyst proliferation seen in $\Delta patS \Delta hetN$ double mutants [40], which we do not attempt to address without carbohydrate dynamics.

3.6. Heterocyst spacings with $\Delta hetN$

Experimental filaments without lateral inhibition due to *hetN* exhibit a wild-type heterocyst pattern at 24 h, but a Mch phenotype at 48 h [20].

As illustrated in figure 2, local effects of $\Delta hetN$ in the model arise because of the gap of duration τ_S between the end of lateral inhibition due to *patS* and the start of lateral inhibition due to nitrogen fixation by the mature heterocyst. Figures 5(*e*) and (*f*) show the model heterocyst spacing distributions at 24 and 48 h for filaments without HetN type inhibition. At 24 h the distribution is similar to the wild type distribution of figure 4(*a*), but at 48 h we see a Mch phenotype as well as a significant number of shorter spacings between heterocysts. In figure 3(*c*) the $\Delta hetN$ heterocyst frequency approximately follows the WT frequency until about 28 h, when it begins to again rapidly increase to a peak of 16.4% at 42 h. This large excess of heterocysts causes the frequency to subsequently
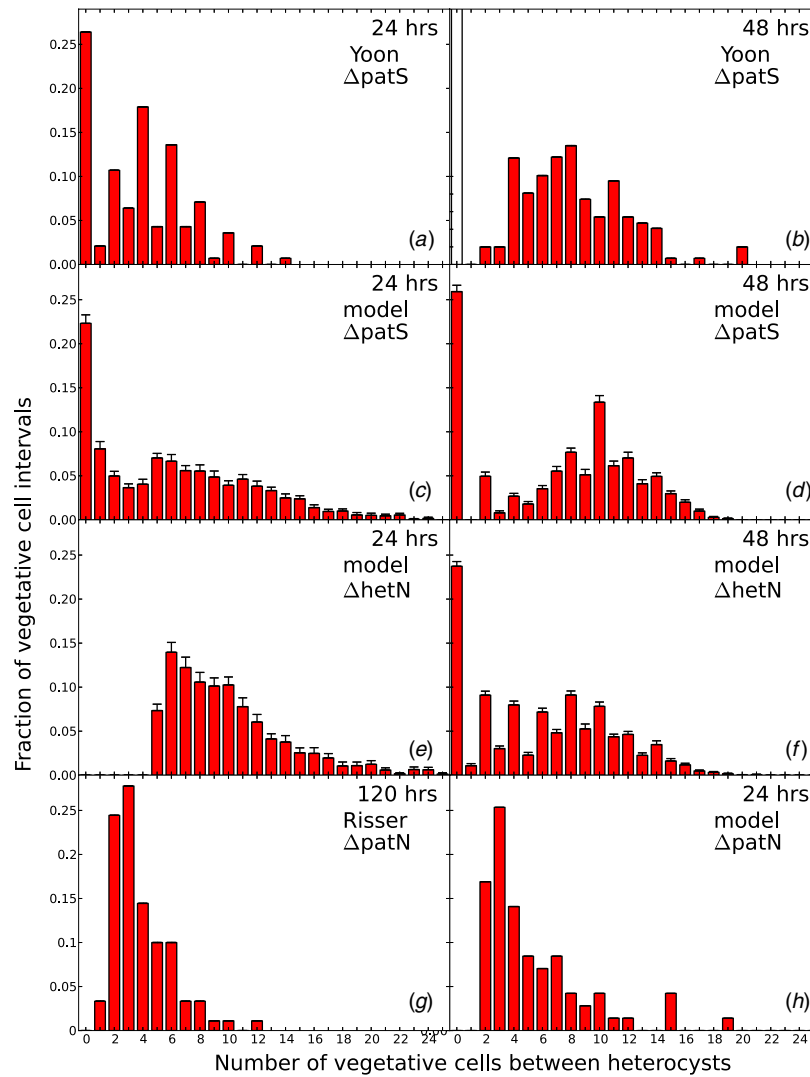
Figure 5. Heterocyst spacing distributions for inhibition mutants. Experimental Δ*patS* PCC 7120 from Yoon and Golden [5, 19] is shown in (*a*) and (*b*) with distributions at 24 h and 48 h as indicated. Experimental zero-spacing data at 48 h was not reported [5], so is represented by an unfilled bar. Model results for Δ*patS* are shown in (*c*) and (*d*). Model results for Δ*hetN* are shown in (*e*) and (*f*). Experimental Δ*patN* *Nostoc punctiforme* ATCC 29133 data from figure S1(A) of Risser *et al* [22] is shown in (*g*). Model results for an inhibition range of two cells are shown in (*h*).

drop to below the WT frequency before again increasing, showing an oscillation of much greater period and amplitude than either WT or Δ*patS*. Heterocyst frequency versus time for *Anabaena* PCC 7120 with *hetN* transcription inactivated is very similar to wild-type for 24 h, increasing to approximately 20% at 48 h, and seems to slowly oscillate while increasing after 48 h [40]. The model has a smaller peak, and misses the subsequent slow increase, which we believe is due to its lack of carbohydrate dynamics.

Variation of the duration of the inhibition gap τ_S did not significantly affect model results (see figure S3, we use $\tau_S = \tau_N = 1$ h). Essentially, any non-zero gap allows fN-depleted cells to commit. Despite the inhibition gap, newly committed cells will laterally inhibit their neighbors via *patS*—so not all cells will commit, even though many vegetative cells have depleted nitrogen storage at 18–24 h. This leads to a significant difference between heterocyst clusters we see in Δ*patS* and those we see in Δ*hetN*. Heterocyst clusters in

Δ*patS* occur because cells commit beside one another roughly at the same time—neighboring heterocysts are in the same generation. Conversely, heterocyst clusters in Δ*hetN* cannot arise this way because lateral inhibition due to *patS* prevents it. Rather, in Δ*hetN* heterocyst clusters arise because new heterocysts commit adjacent to older, mature heterocysts.

3.7. Heterocyst spacings with Δ*patN*

Filaments of *Nostoc punctiforme* ATCC 29133 lacking *patN* have an altered heterocyst pattern, with more heterocysts, as shown in figure 5(*g*) [22]. While patterned expression of *patN* may also influence the heterocyst pattern [22], we use the model to explore how much the reported heterocyst pattern may arise simply from decreasing the range of PatS and HetN inhibition.

Figure S1(B) of Risser *et al* [22] indicates that significant nitrogen fixation and growth is only just starting at 120 h,
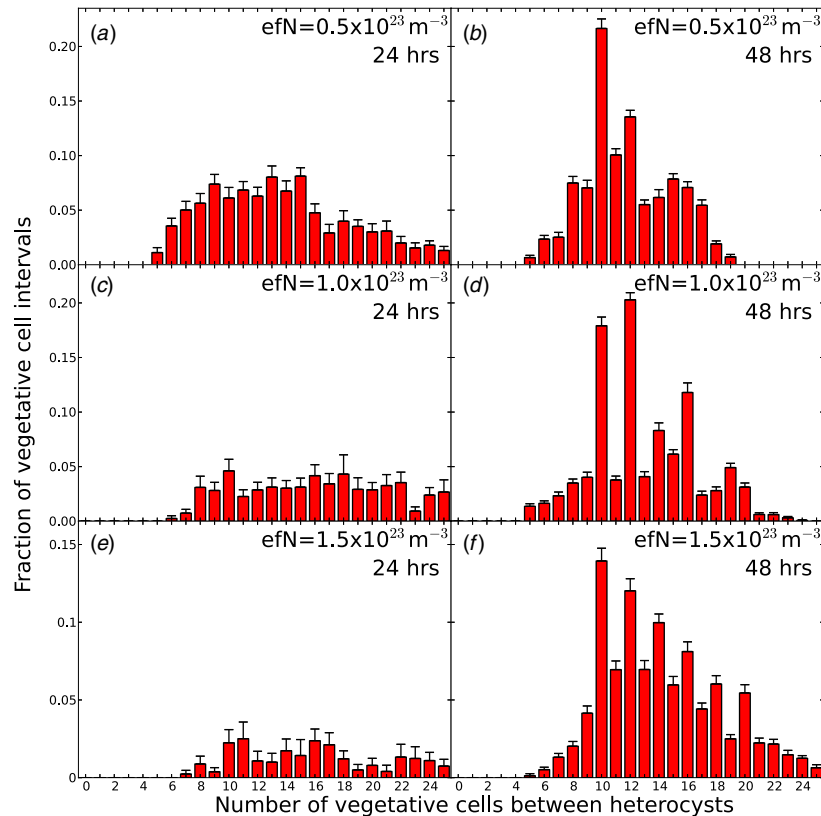
Figure 6. Wild-type heterocyst spacing distributions for different stepped down external fixed nitrogen (efN) concentrations. (*a*) and (*b*) spacing distribution at 24 h and 48 h, respectively, with efN concentration of 0.5×10^{23} m^{-3} (see ρ_{efN} in equation (1)). (*c*) and (*d*) spacing distribution at 24 h and 48 h, respectively, with efN concentration of 1.0×10^{23} m^{-3}. (*e*) and (*f*) spacing distribution at 24 h and 48 h, respectively, with efN concentration of 1.5×10^{23} m^{-3}.

when the heterocyst spacing distribution was measured. In figure 5(*h*) we show the heterocyst spacing distribution using the model for an inhibition range of two cells after 24 h. This corresponds to when nitrogen fixation and growth starts again due to heterocyst maturation. We find that the heterocyst spacing distribution from the model with an inhibition range of two cells and the experimental Δ*patN* heterocyst spacing distribution are similar. This suggests that shortened inhibition ranges from PatS and HetN may play a role in shaping the Δ*patN* phenotype.

3.8. Non-zero external fixed nitrogen concentrations

Since local fN is an important part of local heterocyst placement in the model, we expect non-zero external fN levels to change both the heterocyst spacing distribution and heterocyst frequency. This was observed with a simpler computational model that was limited to steady-state growth, long after fN step-down [7].

Figure 3(*d*), which shows the heterocyst frequency versus time, illustrates that strong relative differences can arise at around 24 h due to slight differences in commitment timing. Figure 3(*d*) also recovers the previous result [7] that at later times the heterocyst frequency decreases as the external fN increases. At the highest external fN concentration shown, 1.5×10^{23} m^{-3}, the late time heterocyst frequency is still nearly 5%. In contrast, we find that at 2.0×10^{23} m^{-3}, the heterocyst frequency does not rise above 1%.

We also observe that the oscillation of heterocyst numbers can lead to quite similar heterocyst percentages for significantly different levels of external fN. To illustrate this effect, in figure 6, we show heterocyst spacing distributions from the model at 24 and 48 h after fN step-down for three non-zero external fN concentrations. We see that relative differences in the spacing distributions are larger at 24 h than at 48 h, reflecting similar differences in heterocyst frequencies.

Thiel and Pratte [23] observed regular patterning of heterocysts in strains with vegetative cells expressing nitrogenase and producing fN under anoxic conditions. The nitrogenase in vegetative cells appeared after 2 h of nitrogen deprivation, implying this fN was supplied prior to the typical commitment times that begin at 8 h [5]. Since we find that both heterocyst frequencies and heterocyst patterns do not dramatically change with moderate levels of non-heterocystous fN (in the case of the model, initially external to the filament), or even quite large levels of external fN at particular time points, we caution that the results of Thiel and Pratte may not rule out a storage-based heterocyst commitment model with a significant role for local fN in local heterocyst placement.

4. Summary

We have developed a dynamic developmental model of heterocystous cyanobacterial filaments that captures both

the early and late heterocyst frequencies and spacings, in both wild-type filaments and in Δ*patS* and Δ*hetN* mutants. The computational model incorporates fN storage with fN transport, cell growth and division, and explicit lateral inhibition with heterocyst commitment and development.

Initial commitment of heterocysts is significantly delayed after the removal of fN in the extracellular medium [5, 33], but the broad timing of commitment indicated by earlier experimental results shown in figure 3(*a*) implies significant stochasticity in the commitment process. The model is deliberately as deterministic as possible; the only source of stochasticity is modest growth rate variability [7, 25] needed for a natural population structure that properly samples the entire range of cell sizes. Since the model recovers both heterocyst spacing and the distribution of the timing of commitment, we have shown that population context [21] is alone sufficient to explain observed patterns of heterocyst commitment. The commitment model is similar to a proposed two-stage model [27], with biased initiation relying upon storage levels rather than cell-cycle position.

Although it has been reported that only small newly divided daughter cells can differentiate into heterocysts [8, 9, 42], recent reports are clear that division is not a requirement for heterocyst differentiation [10, 11]. Indeed, cell-lineage studies show that even inhibition of division leads to elongated heterocysts [11] rather than suppressing them altogether. Nevertheless, it appears that cell-cycle and the cell-fate decision to develop into a heterocyst are correlated.

Using our model, we examine the statistics of how heterocyst differentiation is related to cell size, since size is closely linked to the cell cycle in living cells. A strong indirect cell cycle commitment effect, seen in figure 3(*b*), arises in the model from a uniform density of available storage determining a total storage that varies with cell size: smaller cells have less stored nitrogen. Because cell growth rates are not cell-size dependent in our model, smaller cells will typically exhaust their storage and commit earlier than larger cells. These cells then laterally inhibit other cells. This increased likelihood of small cells to differentiate into heterocysts due to more-rapid local depletion of storage offers an alternative explanation for a relationship between heterocyst differentiation and recent cell division. With the natural population structure of cell sizes in the filament, we believe that this explains the observed distribution of commitment times. With lateral inhibition, this then allows different cell-fate decisions—breaking the apparent initial symmetry of a clonal filament of vegetative cells. This commitment model, in which commitment follows local storage depletion, predicts that higher filamentous growth rate, as modulated by e.g. light intensity [11, 43], should lead to earlier commitment, as illustrated in figure 3(*a*). We also expect that strains with less fN storage, such as strains without cyanophycin [44], with a correspondingly smaller f_s in the model, should have significantly earlier commitment and correspondingly earlier heterocyst differentiation.

Lateral inhibition from committed and mature heterocysts, due to *patS* [5, 19] and *hetN* [20] respectively, is necessary to achieve the wild-type heterocyst pattern. Without *patS* inhibition that occurs upon commitment, cells can commit

nearby one another and the 24 h pattern exhibits Mch and very short spacings between heterocysts. Without *hetN* inhibition, the initial heterocyst pattern is qualitatively unchanged. However any temporal gap in the inhibition from a maturing heterocyst between *patS* and newly synthesized fN (τ_S in figure 2) will lead to Mch and short spacings at 48 h. Because *patS* continues to prevent simultaneous commitment of new heterocyst clusters, the Mch clusters seen in Δ*hetN* are always built around older heterocysts in the model. This is both a novel prediction of, and a natural consequence of, the model. We also found that reducing the inhibition range of *patS* and *hetN* to two cells yielded a heterocyst pattern similar to that of Δ*patN* [22] filaments (see section 3.7 and figures 5(*g*) and (*h*)).

Motivated by the observation of qualitatively unchanged heterocyst development despite ongoing nitrogen fixation in vegetative cells under anoxic conditions [23], we investigated step-down to nonzero external fN concentrations. After stepping down to nonzero external fN concentrations, no dramatic changes were seen in the modeled heterocyst pattern, frequency, and differentiation timing until the external fN nearly suppressed heterocysts altogether. This is particularly true at intermediate times after fN step-down. This suggests that our model of heterocyst commitment due to local fN levels may be consistent with the experimental observation of heterocysts despite nitrogen fixation in vegetative cells under anoxic conditions. Quantitative agreement of model and experimental patterns will require characterization of fN sources, sinks, transport and storage, as well as stochastic cellular growth.

As more detailed spatial and temporal patterns of expression of patterning genes are forthcoming, they can be more accurately represented in the model. Some refinements of the model are already suggested from the artificially sharp inhibition range built into the model and evident in figure 4 compared with experimental short-range spacings. We have also noted that carbohydrate dynamics, with sources in vegetative cells and sinks in heterocysts, may be needed when heterocyst frequencies exceed those of WT.

The developmental model, summarized in figure 2, is deliberately simplified. It is deterministic, or hierarchical [18], after initial commitment. Subsequent lateral inhibition is Boolean (on or off) in character [37], and of fixed range. We know that the details of the biological regulatory network of lateral inhibition and commitment are much more complex [1, 2]. Nevertheless, while many 'patterning' genes have been identified that change heterocyst patterns when perturbed, their mechanism of action is sometimes less clear [1]. We believe that the less-visible landscape of metabolites must be taken into account while determining mechanisms of patterning gene action. For the model of heterocyst development in cyanobacterial filaments, we emphasize the role of fN and especially of fN storage in determining the observed developmental pattern. This is consistent with the increasingly prominent role played by metabolic gradients in determining patterns of multicellular development in bacterial systems (see, e.g., [45]).

Nevertheless, a key question is how the expression of patterning genes correlates with subsequent heterocyst

development, both spatially and temporally. In particular, how variable is the timing and strength of expression of inhibition factors from cells that subsequently develop into heterocysts? The model, with hierarchic timing and Boolean expression after commitment, can explain observed heterocyst patterns. Whether this indicates similarly hierarchic timing *in vivo*, or simply robustness of the spacing distributions to additional experimental stochasticities, remains to be determined.

There remains considerable experimental uncertainty in almost all of the parameters used in the model. We have tried to explicitly avoid fine-tuning of parameters by being clear about the reasoning and experimental data involved in determining the parameters. Nevertheless, appropriate model parameters are expected to depend on experimental growth conditions, as well as the cyanobacterial species and strain or mutant used. A detailed understanding of phenotypic heterocyst patterning differences with varying experimental conditions will probably require identification and measurement of significant corresponding parameter differences. We expect that growth rates and nitrogen storage dynamics will be among these significant parameters, and that related parameters should be characterized whenever possible.

Acknowledgments

References

[1] Flores E and Herrero A 2010 Compartmentalized function through cell differentiation in filamentous cyanobacteria *Nature Rev. Microbiol.* **8** 39–50

[2] Kumar K, Mella-Herrera R A and Golden J W 2010 Cyanobacterial heterocysts *Cold Spring Harb. Perspect. Biol.* **2** a000315

[3] Wolk C P 1996 Heterocyst formation *Annu. Rev. Genet.* **30** 59–78

[4] Laurent S, Chen H, Bedu S, Ziarelli F, Peng L and Zhang C 2001 Nonmetabolizable analogue of 2-oxoglutarate elicits heterocyst differentiation under repressive conditions in *Anabaena* sp. PCC 7120 *Arch. Microbiol.* **176** 9–18

[5] Yoon H and Golden J W 2001 PatS and products of nitrogen fixation control heterocyst pattern *J. Bacteriol.* **183** 2605–13

[6] Mullineaux C W, Mariscal V, Nenninger A, Khanum H, Herrero A, Flores E and Adams D G 2008 Mechanism of intercellular molecular exchange in heterocyst-forming cyanobacteria *EMBO J.* **27** 1299–308

[7] Brown A I and Rutenberg A D 2012 Reconciling cyanobacterial fixed-nitrogen distributions and transport experiments with quantitative modelling *Phys. Biol.* **9** 016007

[8] Mitchison G J, Wilcox M and Smith R J 1976 Measurement of an inhibitory zone *Science* **191** 866–8

[9] Sakr S, Jeanjean R, Zhang C and Arcondeguy T 2006 Inhibition of cell division suppresses heterocyst development in *Anabaena* sp. strain PCC 7120 *J. Bacteriol.* **188** 1396–404

[10] Asai H, Iwamori S, Kawai K, Ehira S, Ishihara J, Aihara K, Shoji S and Iwasaki H 2009 Cyanobacterial cell lineage

[11] Toyoshima M, Sasaki N V, Fujiwara M, Ehira S, Ohmori M and Sato N 2010 Early candidacy for differentiation into heterocysts in the filamentous cyanobacterium *Anabaena* sp. PCC 7120 *Arch. Microbiol.* **192** 23–31

[12] Nachman I, Regev A and Ramanathan S 2007 Dissecting timing variability in yeast meiosis *Cell* **131** 544–56

[13] St-Pierre F and Endy D 2008 Determination of cell fate selection during phage lambda infection *Proc. Natl Acad. Sci. USA* **105** 20705–10

[14] Li H, Sherman D M, Bao S and Sherman L A 2001 Pattern of cyanophycin accumulation in nitrogen-fixing and non-nitrogen-fixing cyanobacteria *Arch. Microbiol.* **176** 9–18

[15] Bogorad L 1975 Phycobiliproteins and complementary chromatic adaptation *Annu. Rev. Plant Physiol.* **26** 369–401

[16] Allen M M 1984 Cyanobacterial cell inclusions *Annu. Rev. Microbiol.* **38** 1–25

[17] Buikema W J and Haselkorn R 1993 Molecular genetics of cyanobacterial development *Annu. Rev. Plant Physiol. Plant Mol. Biol.* **44** 33–52

[18] Buganim Y, Faddah D A, Cheng A W, Itskovich E, Markoulaki S, Ganz K, Klemm S L, van Oudenaarden A and Jaenisch R 2012 Single-cell expression analyses during cellular reprogramming reveal an early stochastic and a late hierarchic phase *Cell* **150** 1209–22

[19] Yoon H and Golden J W 1998 Heterocyst pattern formation controlled by a diffusible peptide *Science* **282** 935–8

[20] Callahan S M and Buikema W J 2001 The role of HetN in maintenance of the heterocyst pattern in *Anabaena* sp. PCC 7120 *Mol. Microbiol.* **40** 941–50

[21] Snijder B, Sacher R, Ramo P, Damm E, Liberali P and Pelkmans L 2009 Population context determines cell-to-cell variability in endocytosis and virus infection *Nature* **461** 520–3

[22] Risser D D, Wong F C Y and Meeks J C 2012 Biased inheritance of the protein patN frees vegetative cells to initiate patterned heterocyst differentiation *Proc. Natl Acad. Sci. USA* **109** 15342–7

[23] Thiel T and Pratte B 2001 Effect on heterocyst differentiation of nitrogen fixation in vegetative cells of the cyanobacterium *Anabaena variabilis* ATCC 29413 *J. Bacteriol.* **183** 280–6

[24] Wolk C P, Austin S M, Bortins J and Galonsky A 1974 Autoradiographic localization of ^{13}N after fixation of ^{13}N-labeled nitrogen gas by a heterocyst-forming blue-green alga *J. Cell Biol.* **61** 440–53

[25] Allard J F, Hill A L and Rutenberg A D 2007 Heterocyst patterns without patterning proteins in cyanobacterial filaments *Dev. Biol.* **312** 427–34

[26] Brown A I and Rutenberg A D 2012 Heterocyst placement strategies to maximize the growth of cyanobacterial filaments *Phys. Biol.* **9** 046002

[27] Meeks J C and Elhai J 2002 Regulation of cellular differentiation in filamentous cyanobacteria in free-living and plant-associated symbiotic growth states *Microbiol. Mol. Biol. Rev.* **66** 94–121

[28] Wolk C P and Quine M P 1975 Formation of one-dimensional patterns by stochastic processes and by filamentous blue-green algae *Dev. Biol.* **46** 370–82

[29] Zhu M, Callahan S M and Allen J S 2010 Maintenance of heterocyst patterning in a filamentous cyanobacterium *J. Biol. Dyn.* **4** 621–33

[30] Picossi S, Montesinos M L, Pernil R, Lichtle C, Herrero A and Flores E 2005 ABC-type neutral amino acid permease N-I is required for optimal diazotrophic growth and is

repressed in the heterocysts of *Anabaena* sp. strain PCC 7120 *Mol. Microbiol.* **57** 1582–92

[31] Reshes G, Vanounou S, Fishov I and Feingold M 2008 Cell shape dynamics in *Escherichia coli Biophys. J.* **94** 251–64

[32] Picossi S, Valladares A, Flores E and Herrero A 2004 Nitrogen-regulated genes for the metabolism of cyanophycin, a bacterial nitrogen reserve polymer *J. Biol. Chem.* **279** 11582–92

[33] Bradley S and Carr N G 1976 Heterocyst and nitrogenase development in *Anabaena cylindrica J. Gen. Microbiol.* **96** 175–84

[34] Golden J W, Whorff L L and Wiest D R 1991 Independent regulation of *nifHDK* operon transcription and DNA rearrangement during heterocyst differentiation in the cyanobacterium *Anabaena* sp. strain PCC 7120 *J. Bacteriol.* **173** 7098–105

[35] Higa K C, Rajagopalan R, Risser D D, Rivers O S, Tom S K, Videau P and Callahan S M 2012 The RGSGR amino acid motif of the intercellular signalling protein, HetN, is required for patterning of heterocysts in *Anabaena* sp. strain PCC 7120 *Mol. Microbiol.* **83** 682–93

[36] Bauer C C, Ramaswamy K S, Endley S, Scappino L A, Golden J W and Haselkorn R 1997 Suppression of heterocyst differentiation in *Anabaena* PCC 7120 by a cosmid carrying wild-type genes encoding enzymes for fatty acid synthesis *FEMS Microbiol. Lett.* **151** 23–30

[37] Fisher J and Henzinger T A 2007 Executable cell biology *Nature Biotechnol.* **25** 1239–49

[38] Risser D D and Callahan S M 2009 Genetic and cytological evidence that heterocyst patterning is regulated by inhibitor gradients that promote activator decay *Proc. Natl Acad. Sci. USA* **106** 19884–8

[39] Bohme H and Haselkorn R 1988 Molecular cloning and nucleotide sequence analysis of the gene coding for heterocyst ferrodoxin from the cyanobacterium *Anabaena* sp. strain PCC 7120 *Mol. Gen. Genet.* **214** 278–85

[40] Borthakur P B, Orozco C C, Young-Robbins S S, Haselkorn R and Callahan S M 2005 Inactivation of *patS* and *hetN* causes lethal levels of heterocyst differentiation in the filamentous cyanobacterium *Anabaena* sp. PCC 7120 *Mol. Microbiol.* **57** 111–23

[41] Murry M A and Wolk C P 1989 Evidence that the barrier to the penetration of oxygen into heterocysts depends upon two layers of the cell envelope *Arch. Microbiol.* **151** 469–74

[42] Adams D G and Carr N G 1981 The developmental biology of heterocyst and akinete formation in cyanobacteria *Crit. Rev. Microbiol.* **9** 45–100

[43] Neunuebel M R and Golden J W 2008 The *Anabaena* sp. strain PCC 7120 gene all2874 encodes a diguanylate cyclase and is required for normal heterocyst development under high-light growth conditions *J. Bacteriol.* **190** 6829–36

[44] Ziegler K, Stephan D P, Pistorius E K, Ruppel H G and Lockau W 2001 A mutant of the cyanobacterium *Anabaena variabilis* ATCC 29413 lacking cyanophycin synthetase: growth properties and ultrastructural aspects *FEMS Microbiol. Lett.* **196** 13–18

[45] Serra D O, Richter A M, Klauck G, Mika F and Hengge R 2013 Microanatomy at cellular resolution and spatial order of physiological differentiation in a bacterial biofilm *mBio* **4** e00103–13